ACS APPLIED MATERIALS & INTERFACES

www.acsami.org

Research Article

Ultrasmall Self-Cascade AuNP@FeS Nanozyme for H_2S-Amplified Ferroptosis Therapy

Jiezhao Zhan, Jianping Liu, Jing Yang, Lin Huang, Yudie Lu, Xuanyi Lu, Jiaoyang Zhu, Sugeun Yang,* and Zheyu Shen*

Cite This: *ACS Appl. Mater. Interfaces* 2023, 15, 46213−46225

Read Online

ACCESS | Metrics & More | Article Recommendations | Supporting Information

ABSTRACT: Recently, nanozymes with peroxidase (POD)-like activity have shown great promise for ferroptosis-based tumor therapy, which are capable of transforming hydrogen peroxide (H_2O_2) to highly toxic hydroxyl radicals (•OH). However, the unsatisfactory therapeutic performance of nanozymes due to insufficient endogenous H_2O_2 and acidity at tumor sites has always been a conundrum. Herein, an ultrasmall gold (Au) @ ferrous sulfide (FeS) cascade nanozyme (AuNP@FeS) with H_2S-releasing ability constructed with an Au nanoparticle (AuNP) and an FeS nanoparticle (FeSNP) is designed to increase the H_2O_2 level and acidity in tumor cells *via* the collaboration between cascade reactions of AuNP@FeS and the biological effects of released H_2S, achieving enhanced •OH generation as well as effective ferroptosis for tumor therapy. The cascade reaction in tumor cells is activated by the glucose oxidase (GOD)-like activity of AuNP in AuNP@FeS to catalyze intratumoral glucose into H_2O_2 and gluconic acid; meanwhile, the released H_2S from AuNP@FeS reduces H_2O_2 consumption by inhibiting intracellular catalase (CAT) activity and promotes lactic acid accumulation. The two pathways synergistically boost H_2O_2 and acidity in tumor cells, thus inducing a cascade to generate abundant •OH by catalyzing H_2O_2 through the POD-like activity of FeS in AuNP@FeS and ultimately causing amplified ferroptosis. *In vitro* and *in vivo* experiments demonstrated that AuNP@FeS presents a superior tumor therapeutic effect compared to that of AuNP or FeS alone. This strategy represents a simple but powerful method to amplify ferroptosis with H_2S-releasing cascade nanozymes and will pave a new way for the development of tumor therapy.

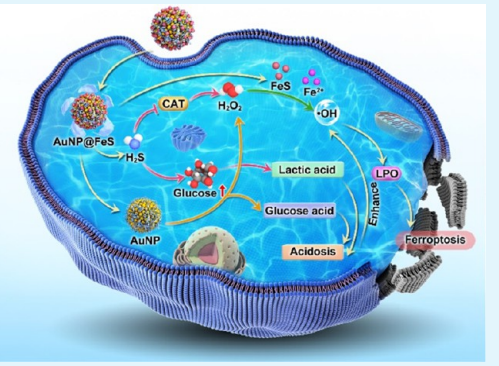

KEYWORDS: *ferroptosis therapy, gas therapy, cascade nanozymes, catalytic therapy, acidosis*

INTRODUCTION

Ferroptosis is a new type of cell death, which is iron-dependent with overaccumulation of reactive oxygen species (ROS), leading to lipid peroxidation accumulation and cell death.[1−3] This unique cell death could destroy drug-resistant cells, presenting a broad development prospect in tumor therapy.[4] To achieve high-performance ferroptosis, a high level of intracellular ROS is one of the most fundamental requirements. Due to the ability to generate abundant ROS with high efficiency, peroxidase (POD)-like *iron*-based nanozymes, which can catalyze H_2O_2 into hydroxyl radicals (•OH, a highly toxic ROS), have attracted significant interest for ferroptosis therapy in recent years.[5] Meanwhile, the hydrogen peroxide (H_2O_2) and weak acidity in the tumor microenvironment (TME) play a pivotal role during the process of tumor therapy owing to facilitating •OH generation and further inspire researchers to construct tumor microenvironment-activatable nanoenzymes for enhancing tumor therapeutic effects by combining with chemotherapy,[6] photodynamic therapy,[7] and sonodynamic therapy.[8] However, the hydrogen peroxide (H_2O_2) and acidity in TME are still insufficient to induce the sustained large production of •OH,[9,10] limiting the therapeutic of nanozyme-based ferroptosis. Therefore, strategies to promote H_2O_2 level and acidity in TME to facilitate the catalytic performance of POD-like nanozymes are of high importance for ferroptosis-based tumor therapy.

Cascade platforms, which are constructed with different enzyme-like activities, are a promising method to regulate H_2O_2 and acidity in TME.[11] Gold nanoparticle (AuNP) with glucose oxidase (GOD)-like activity (Au nanozyme), which can catalyze the overexpressed glucose in TEM into H_2O_2 and gluconic acid, has great potential to boost H_2O_2 supply and regulate acidity.[12,13] For example, Shi et al. constructed a cascade nanozyme based on Au nanozymes and ferroferric oxide (Fe_3O_4) nanozymes on a mesoporous silica catalytic platform to generate H_2O_2 and gluconic acid, promoting •OH generation of Fe_3O_4 nanozymes.[14] Wang et al. constructed a

Received: June 23, 2023
Accepted: September 10, 2023
Published: September 23, 2023

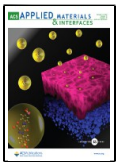

Scheme 1. (a) Illustration for the Construction of the AuNP@FeS Nanozyme. (b) Schematic Illustration of the Antitumor Mechanism of the AuNP@FeS Nanozyme by H_2S-Amplified Ferroptosis

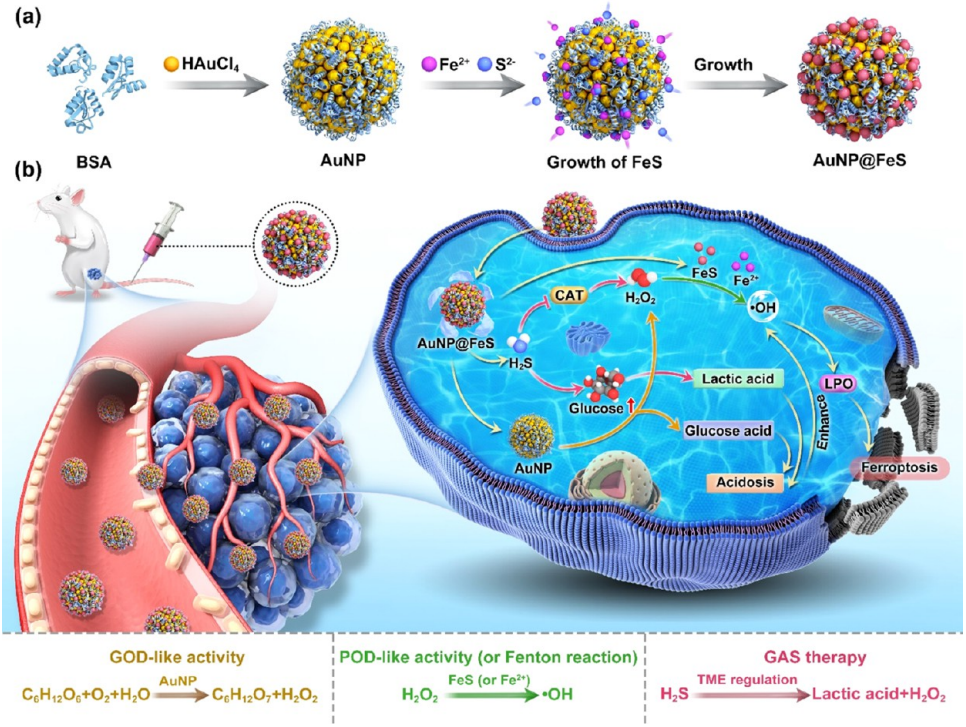

cascade platform with manganese-doped hollow mesoporous silica-coated Au nanozymes to supply H_2O_2 and gluconic acid for Mn^{2+} to generate $^{\bullet}OH$, enhancing the effect of tumor treatment.[15] Although these strategies make an important contribution to increasing the intracellular H_2O_2 level and acidity, they are still limited and face a huge challenge due to the intracellular defense system and tumor metabolism. As the representative of the intracellular defense system, catalase (CAT) is excessively expressed in tumor cells, which can consume H_2O_2 and decrease the free $^{\bullet}OH$ content, inducing an unsatisfactory therapeutic effect.[16,17] Although gluconic acid can enhance the acidity, gluconic acid is not the main cause of tumor acidification. Indeed, tumor cells consume glucose and convert it into large amounts of lactic acid through the Warburg metabolic process,[18,19] which is one of the main causes of tumor acidification and an important method of regulating acidity. Thus, seeking an adaptive strategy to increase H_2O_2 and acidity by constructing cascade platforms with CAT inhibiting ability and lactic acid regulation is highly imperative for ferroptosis therapy.

As an endogenous gas signaling molecule, hydrogen sulfide (H_2S) exists in mammals and plays an important role in a variety of physiological and pathophysiological processes.[20] Recently, a novel "gas" therapy based on H_2S has proved to be an effective tumor suppressor with minimal side effects.[21] It is worth noting that H_2S holds the ability to inhibit CAT activity in tumor cells, thus reducing the expenditure of endogenous H_2O_2.[22,23] Moreover, H_2S has been demonstrated to be an efficient approach to regulating lactic acid,[24] which can promote glucose uptake and conversion to lactic acid and inhibit the efflux of protons, enhancing acidification. Inspired by this biochemical event, we intend to combine H_2S gas with the cascade nanozyme for increasing the H_2O_2 level and enhancing acidity in TME as well as for uninterrupted ROS generation. Excitedly, the potential of the H_2S-releasing cascade nanozyme can be achieved by combining with promising ferrous sulfide (FeS) nanoparticles, which can act as donors of both POD activity and H_2S gas. Although several studies have demonstrated the POD activity accompanied by the H_2S-releasing property of FeS nanoparticles (FeSNPs),[25,26] the relatively large particle size (usually 50−200 nm) may hamper its catalytic activity.[27,28]

Inspired by the above thought, we designed ultrasmall (about 2 nm) AuNP@FeS nanozymes by using bovine serum albumin (BSA) as a template. With good biocompatibility, excellent hydrophilicity, and high stability, BSA has become an ideal template for constructing nanozymes with ultrasmall sizes and uniform distribution.[29,30] The as-prepared AuNP@FeS can increase the H_2O_2 concentration *via* opening the source (H_2O_2 self-supply by the GOD activity of Au) and reducing the expenditure (CAT inhibition by released H_2S) and enhance acidity *via* acidosis induced by the synergistic effect of gluconic acid and lactic acid. Collectively, the efficient H_2O_2 generation and acidity enhancement promote the POD-like activity of FeS, thereby boosting $^{\bullet}OH$ for gas-amplified ferroptosis (Scheme 1). In both *in vitro* and *in vivo* experiments, abundant ROS was generated in tumor cells after treatment with H_2S-releasing AuNP@FeS nanozymes. In addition, AuNP@FeS presents good biocompatibility to normal cells, achieving a high tumor therapy effect with biosafety. The combination of H_2S gas therapy and cascade nanozymes can achieve a "1 + 1 > 2" synergistic ferroptosis-based antitumor treatment, providing a new idea for the development of novel combined ferroptosis therapy based on high-performance nanozymes.

https://doi.org/10.1021/acsami.3c09066
ACS Appl. Mater. Interfaces 2023, 15, 46213−46225

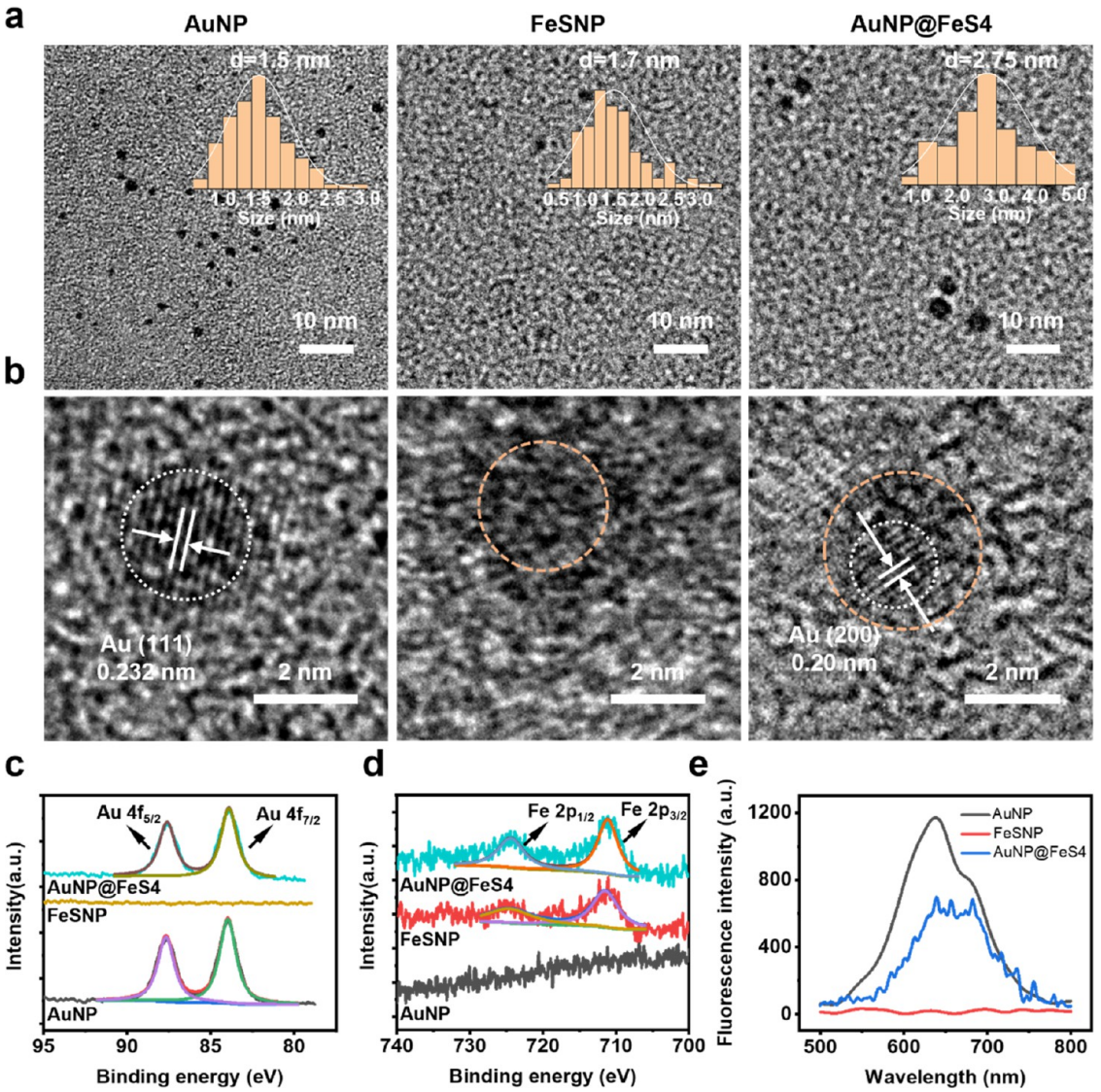

Figure 1. (a, b) Representative TEM morphology (a) and HRTEM (b) of AuNP, FeSNP, and AuNP@FeS4. (c, d) High-resolution XPS spectra of Au 4f (c) and Fe 2p (d) for AuNP, FeSNP, and AuNP@FeS4. (e) Fluorescence spectra of AuNP, FeSNP, and AuNP@FeS4 excited at 480 nm.

RESULTS AND DISCUSSION

Characterization of AuNP@FeS Nanozymes. Au nanoclusters were synthesized *via* the reduction of the BSA template without extra reducing agents. Then, FeS accurately grew on the surface of Au nanoclusters as Fe^{2+} and S^{2-} were diffused into the BSA template, forming AuNP@FeS nanozymes. By adjusting the different feeding mass ratios of Au and Fe (1:0.5, 1:1, 1:2, 1:4, and 1:8), AuNP@FeS nanozymes with different Fe loading contents were prepared (Table S1). The Fe loading contents of AuNP@FeS nanozymes are increased with the feeding mass ratio of Au and Fe. Meanwhile, AuNP@FeS1−4 (prepared with mass ratios of 1:0.5, 1:1, 1:2, and 1:4, respectively) are in a uniform distribution (Figure S1). AuNP@FeS4 with the highest Fe loading content (9.67%) is chosen as the optimal feeding mass ratio as precipitation occurred with the mass ratio of 1:8. The as-prepared AuNP@FeS4 is uniformly distributed with a mean diameter of 2.75 nm, which is slightly greater than those of Au (1.5 nm) and FeSNP (1.7 nm, Figure 1a). Singly synthesized Au nanoclusters present a crystalline structure and FeS is amorphous-structured as a *d*-spacing of 0.232 nm corresponding to the (111) plane of Au[31] and no clear *d*-spacing are observed on high-resolution transmission electron microscopy (HRTEM) images of AuNP and FeSNP (Figure 1b). AuNP@FeS4 presents a *d*-spacing of 0.232 nm corresponding to the (111) plane of Au and an amorphous structure outside the (111) plane, indicating the structure of the Au core and FeS shell. The X-ray photoelectron spectroscopy (XPS) survey spectrum testified to the existence of Fe and Au elements, further proving that AuNP@FeS4 is successfully prepared. The C, N, and O elements on the spectrum are attributed to the BSA template (Figure S2). Then, the high-resolution XPS spectrum was further analyzed for the valence states of Au and Fe in AuNP@FeS4 (Figure 1c,1d). The peaks of Au 4f 5/2 at 87.6 eV and Au 4f 7/2 at 83.9 eV[32] show the existence of Au^0, and Fe 2p1/2 at 711.2 eV and Fe 2p 3/2 at 724.5 eV[33] indicate the existence of Fe^{2+}, indicating good potential in the cascade reaction of GOD-like and POD-like activities, respectively. Meanwhile, the high-resolution XPS spectrum of S 2p was analyzed, and the peaks of S 2p 3/2 at 161.8, 163.6, and 167.5 eV indicate the existence of S−Au, FeS, and organic sulfur species from BSA,[34,35] respectively, further proving the

https://doi.org/10.1021/acsami.3c09066
ACS Appl. Mater. Interfaces 2023, 15, 46213−46225

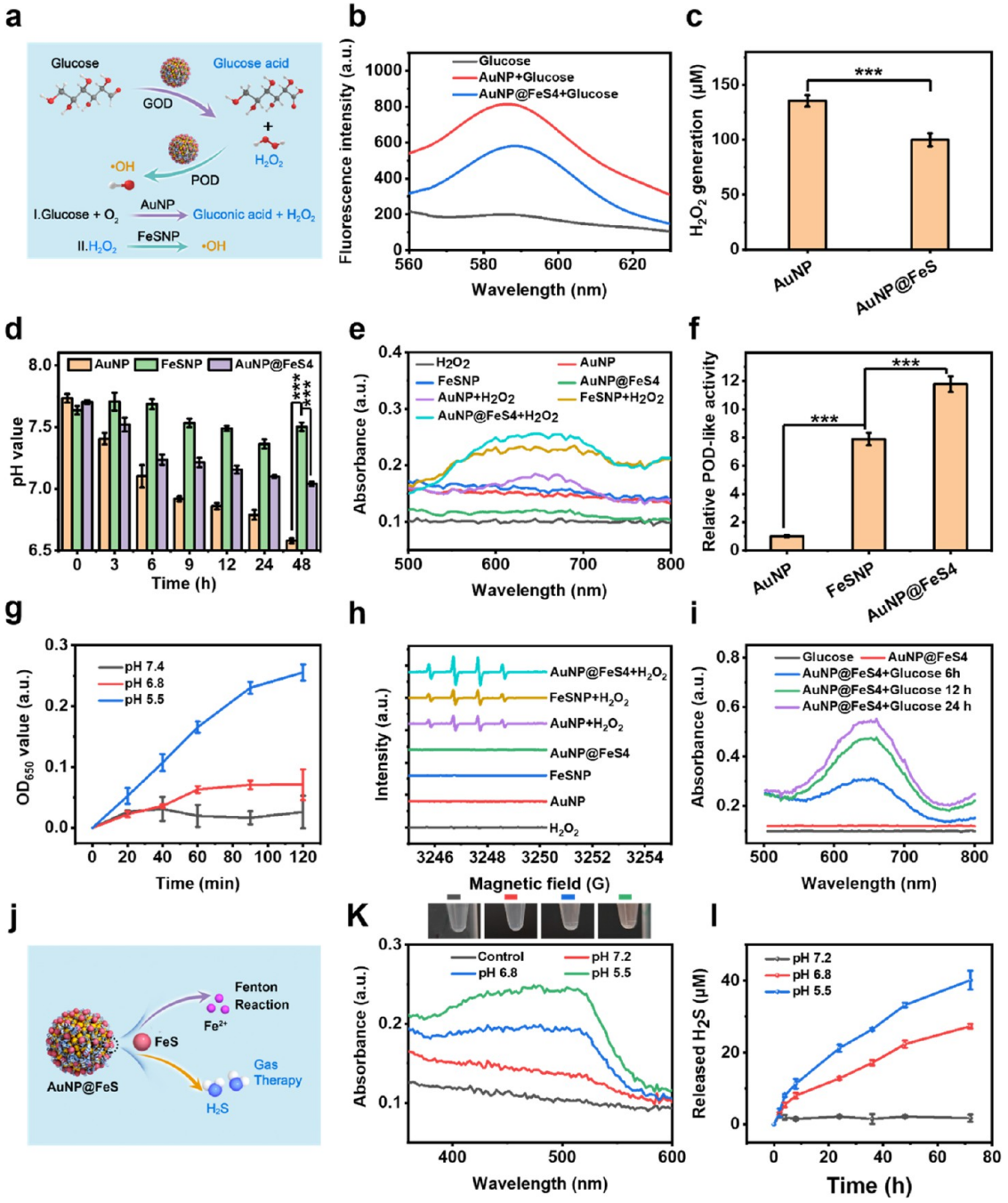

Figure 2. (a) Schematic illustration of the cascade reaction of AuNP@FeS. (b) Fluorescence spectra excited at 540 nm of AuNP, FeSNP, or AuNP@FeS4 with the Amplex red probe after incubation with 5.0 mM glucose for 12 h. (c) H_2O_2 generation of AuNP@FeS4. (d) pH values of AuNP, FeSNP, or AuNP@FeS4 after incubation with 5.0 mM glucose for different times. (e) Ultraviolet−visible (UV−vis) spectra of TMB solutions with H_2O_2, AuNP, FeSNP, AuNP@FeS4, AuNP + H_2O_2, FeSNP + H_2O_2, or AuNP@FeS4 + H_2O_2. (f) Relative POD-like activity of AuNP, FeSNP, and AuNP@FeS4 compared to that of AuNP. (g) Time-dependent UV−vis absorbance of TMB solutions at 650 nm with AuNP@FeS4 and 0.5 mM H_2O_2 at different pH values. (h) ESR spectra of H_2O_2, AuNP, FeSNP, AuNP@FeS4, AuNP + H_2O_2, FeSNP + H_2O_2, or AuNP@FeS4 + H_2O_2 using 5,5-dimethyl-1-pyrroline-*N*-oxide (DMPO) as the $^{\bullet}OH$ trapping agent. (i) UV−vis spectra of TMB solutions with AuNP@FeS4 after incubation with 5.0 mM glucose for different times. (j) Schematic illustration of the Fe^{2+} and H_2S supply behaviors of AuNP@FeS4. (k) UV−vis spectra of o-phenanthroline solutions with degraded solutions of AuNP@FeS4 in different pH environments. (l) Time-dependent H_2S release behaviors of AuNP@FeS4 after incubation at different pH values. ***$P < 0.001$.

formation of AuNP@FeS (Figure S3). As the outer FeS shell hides the inner Au core, AuNP@FeS4 shows a decreased fluorescence intensity as compared to Au nanoclusters (Figure 1e) and presents a ζ-potential similar to that of FeS (Figure S4).

Enzymatic Activity and H_2S Releasing Ability of AuNP@FeS4 Nanozymes. The cascade reactivity of AuNP@FeS4 was constructed by the GOD-like activity of the Au nanozyme and the POD-like activity of the FeS nanozyme (Figure 2a). As a glucose oxidase mimic, the Au nanozyme catalyzes glucose into gluconic acid and H_2O_2[13],

https://doi.org/10.1021/acsami.3c09066
ACS Appl. Mater. Interfaces 2023, 15, 46213−46225

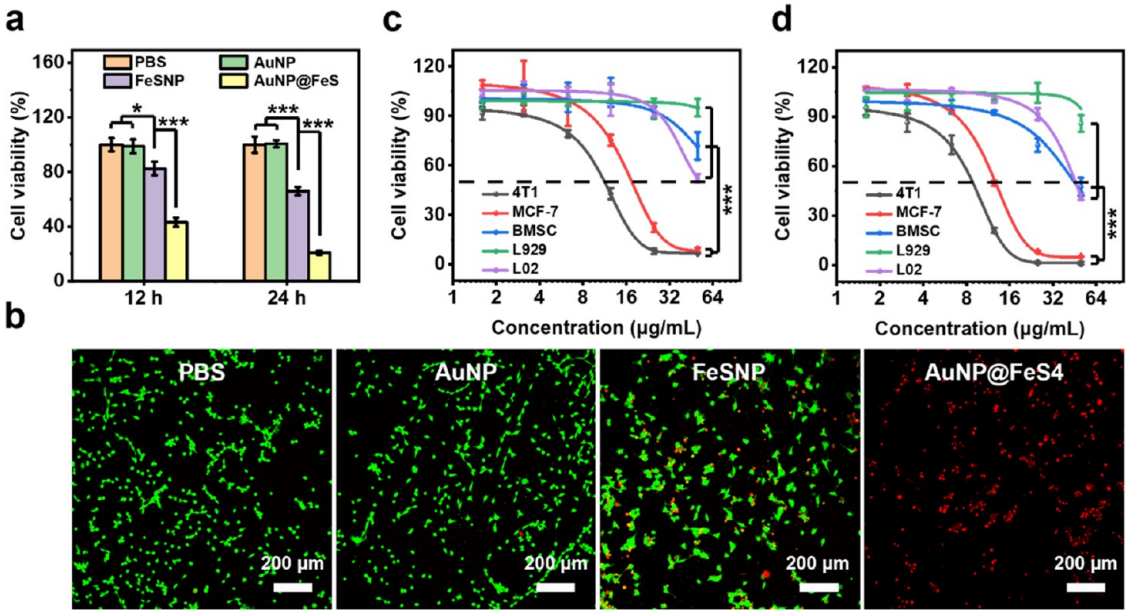

Figure 3. (a) Cell viability of 4T1 cells treated with PBS, AuNP, FeSNP, or AuNP@FeS4. (b) Live/Dead stained images of 4T1 cells treated with PBS, AuNP, FeSNP, or AuNP@FeS4 for 24 h. (c, d) Cell viability of tumor cells and normal cells treated with different concentrations of AuNP@FeS4 for 12 h (c) and 24 h (d). *P < 0.05 and ***P < 0.001.

which not only supplies substrate H_2O_2 but also enhances acidification for the FeS nanozyme to generate $^{\bullet}OH$ *via* the POD-like activity. Therefore, H_2O_2 generation and pH change were detected at first to evaluate the GOD-like activity of Au in AuNP@FeS4. The capacity of H_2O_2 production was detected after AuNP@FeS4 incubation with glucose by using Amplex Red as a probe based on the reaction among Amplex Red, H_2O_2, and HRP, forming resorufin with a maximum emission wavelength at 585 nm.[36] The intensity of the wavelength at 585 nm only slightly decreases in cell lysates compared to no cell lysates, indicating that AuNP presents high and stable GOD-like activity as the GOD-like activity of the Au nanozyme is very sensitive to surface capping[37,38] (Figure S5). The reason why AuNP presents GOD-like activity with BSA modification may be that BSA molecules do not completely cover the Au nanozyme and the exposed Au nanozyme can come in contact with glucose and catalyze glucose.[39] Meanwhile, the maximum emission wavelength appearing at 585 nm indicates that AuNP@FeS4 presents the capacity of the H_2O_2 supply, which is attributed to the GOD-like activity of AuNP (Figure 2b). Although the FeS shell makes AuNP@FeS4 display a lower H_2O_2 supply compared to AuNP, AuNP@FeS4 still can supply H_2O_2 massively in a short time (12 h) owing to the excellent GOD-like activity of AuNP (Figure 2c). Meanwhile, the pH value of the solution was tested after AuNP@FeS4 incubation with glucose (Figure 2d). The decreasing tendency of the pH value corresponds to the GOD-like activity of nanozymes. Owing to the excellent GOD-like activity of AuNP, AuNP@FeS4 can generate gluconic acid and decrease the pH value.

The POD-like activity of AuNP@FeS4 was evaluated with a colorimetric method by using TMB as an indicator (Figure 2e). TMB can be oxidated by $^{\bullet}OH$, forming oxidation TMB with representative UV peaks at 650 nm.[40] AuNP, FeSNP, and AuNP@FeS4 all display POD-like activity, as the representative UV peaks at 650 nm are observed. The quantitative relative POD-like activity was analyzed and is shown in Figure 2f. Compared with AuNP, the relative POD-like activities of FeSNP and AuNP@FeS4 are as high as 7.87 and 11.76 times, indicating that AuNP@FeS4 presents the highest POD-like activity, which contributed to the FeS shell and the Au core as well as the ultrasmall size. Moreover, the POD-like activity of AuNP@FeS4 displays a pH-dependent manner and significantly increases with a decrease in the pH value (Figure 2g). Then, the generated radicals were verified with the spectrum of electron spin resonance (ESR) (Figure 2h). The ESR spectrum shows the peaks with the ratio of 1:2:2:1,[41] further indicating that AuNP@FeS4 catalyzes H_2O_2 to produce $^{\bullet}OH$ and presents the highest POD-like activity among all of the nanozymes.

The above studies demonstrate that AuNP@FeS4 presents a high GOD-like activity and POD-like activity. Then, the cascade activity of AuNP@FeS4 based on the GOD-like activity and POD-like activity was determined after incubation with glucose without extra H_2O_2 by using TMB as the indicator (Figure 2i). The representative peaks at 650 nm indicate that AuNP@FeS4 presents excellent cascade activity, which can efficiently catalyze the conversion of glucose into H_2O_2 and gluconic acid, thus generating $^{\bullet}OH$ sustainably and efficiently. Moreover, AuNP@FeS4 exhibits a time-dependent cascade activity as the absorption is increased with incubation time, which may be attributed to the accumulation of H_2O_2 and gluconic acid during the incubation process.

Because FeS can degrade to Fe^{2+} and H_2S, AuNP@FeS4 is expected to serve as a donor of Fe^{2+} and H_2S (Figure 2j). The Fe^{2+} supply of AuNP@FeS4 was tested with *o*-phenanthroline,[42,43] which can generate a red chelate with a maximum absorption peak at 510 nm by specific binding with Fe^{2+}. The release of Fe^{2+} from AuNP@FeS4 presents acid-responsive behavior as the intensity of the peak at 510 nm increases with the decrease in pH value (Figure 2k), which also can facilitate $^{\bullet}OH$ generation by the Fenton reaction of Fe^{2+}.[44] The H_2S supply of AuNP@FeS4 was explored in different pH environments by detecting with H_2S assay kits. AuNP@FeS4

https://doi.org/10.1021/acsami.3c09066
ACS Appl. Mater. Interfaces 2023, 15, 46213−46225

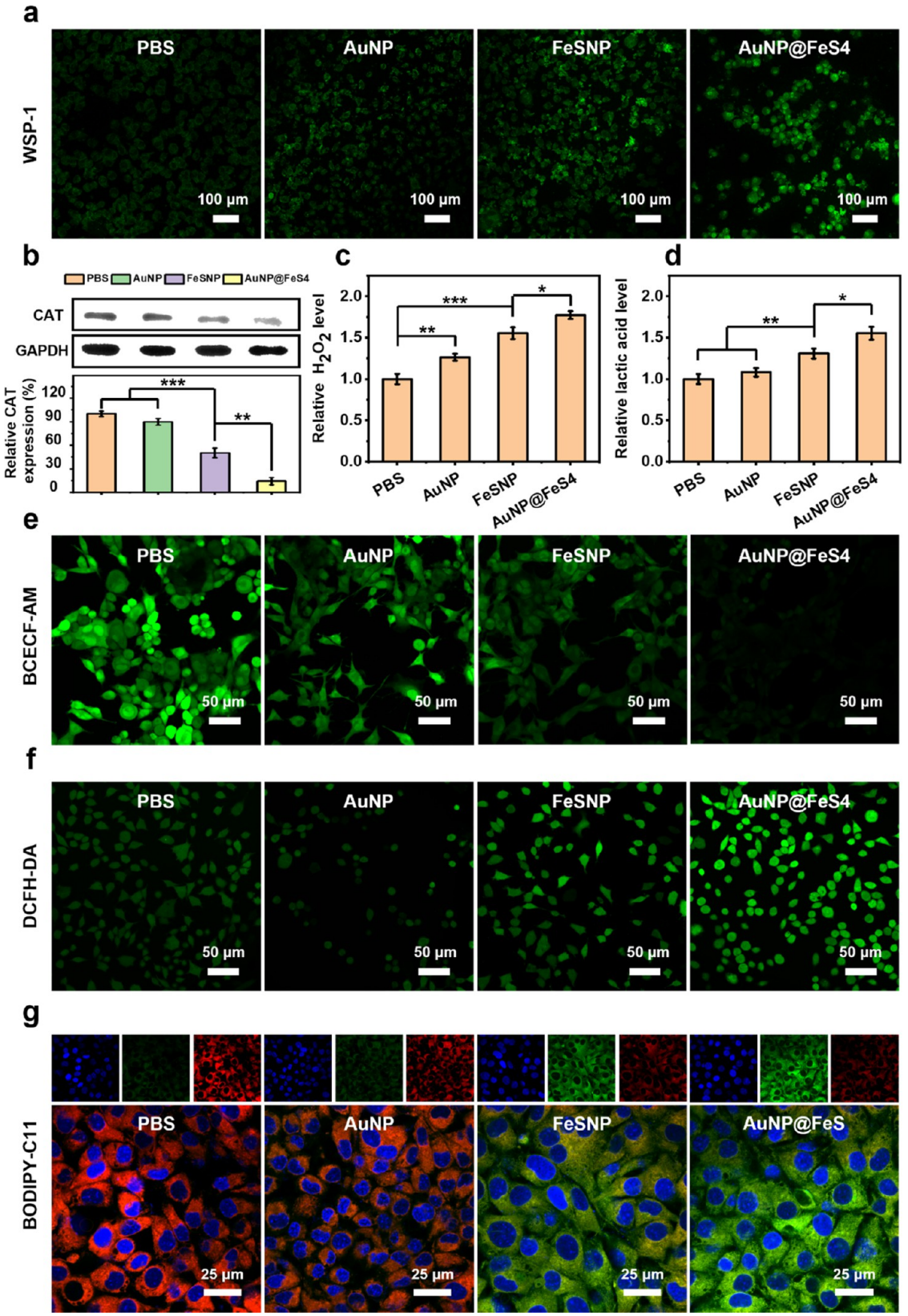

Figure 4. (a) Fluorescence images of intracellular H_2S in 4T1 cells after incubation with PBS, AuNP, FeSNP, or AuNP@FeS4 for 6 h using WSP-1 as the probe. (b) Intracellular CAT expression detected by WB analysis and the corresponding quantitative analysis data calculated from WB analysis. (c) Relative intracellular H_2O_2 level in 4T1 cells after incubation with PBS, AuNP, FeSNP, or AuNP@FeS4 for 12 h. (d) Intracellular lactic acid level in 4T1 cells after incubation with PBS, AuNP, FeSNP, or AuNP@FeS4 for 12 h. (e−g) Intracellular pH fluorescence images (e), ROS fluorescence images (f), and LPO fluorescence images (g) after incubation with PBS, AuNP, FeSNP, or AuNP@FeS4 for 12 h using BCECF-AM, the DCFH-DA probe, or the BODIPY-C11 probe. *P < 0.05, **P < 0.01, and ***P < 0.001.

https://doi.org/10.1021/acsami.3c09066
ACS Appl. Mater. Interfaces 2023, 15, 46213−46225

is stable at pH 7.2 as little H_2S is detected, while it can obviously release a larger amount of H_2S with decreased pH, presenting a pH-dependent H_2S release behavior (Figure 2l). These data demonstrate that AuNP@FeS4 can serve as a H_2S supplier, showing the therapeutic potential of combined gas therapy.

High Antitumor Activity with Good Biocompatibility. The *in vitro* antitumor activity of AuNP@FeS4 was evaluated by the CCK-8 assay (Figure 3a). After a short incubation period of 12 h, AuNP does not kill 4T1 cells, while FeSNP shows a low antitumor activity by killing 17.5% of the 4T1 cells. Meanwhile, AuNP@FeS4 can rapidly kill 56.7% of the 4T1 tumor cells with a low Fe concertation (12.5 μg/mL) during the short incubation period, presenting the best antitumor activity among all groups. The nanozymes present similar antitumor activity trends at 24 h, and AuNP@FeS4 still displays the best antitumor activity, killing 79.1% of the 4T1 cells. The Live/Dead cell staining assay further demonstrates significantly enhanced antitumor activity of AuNP@FeS4 compared to FeSNP and AuNP, as nearly all dead cells (red fluorescence) and little live cells (green fluorescence) are observed in the AuNP@FeS4 group (Figure 3b). Further, the antitumor activity of AuNP, FeNP, and AuNP@FeS4 with different concentrations was evaluated with 4T1 cells (Figure S6). AuNP presents the lowest antitumor activity among all groups and even cannot kill 4T1 cells at a high concentration (100 μg/mL). FeSNP displays a higher antitumor activity as compared to AuNPs, killing 72.7% of the 4T1 cells at 50 μg/mL (Fe content). AuNP@FeS exhibits the highest antitumor activity and kills almost 100% of the 4T1 cells at a relatively low concentration (Fe = 25 μg/mL). These data show that the cascade activity makes AuNP@FeS4 confer its excellent antitumor activity.

The antitumor activity and biocompatibility were further evaluated with two tumor cell lines (4T1 and MCF-7) and three normal cell lines (BMSCs, L929, and L02) at 12 and 24 h with different concentrations of AuNP@FeS4 (Figure 3c,d). The corresponding IC_{50} is listed in Table S2. The IC_{50} values of AuNP@FeS4 for 4T1 and MCF-7 t at 12 h are relatively low to 11.35 and 17.46 μg/mL, respectively, while that was 3−4 times higher for L02 (IC_{50} = 52.52 μg/mL). Notably, the IC_{50} values of AuNP@FeS4 at 12 h for hBMSCs and L929 are undetectable due to good cell viability. In addition, the IC_{50} values of AuNP@FeS4 for all cell lines at 24 h share trends similar to those at 12 h, which are 8.80 and 12.73 μg/mL for 4T1 and MCF-7, respectively, and 45.33, 95.20, and 45.92 μg/mL for BMSCs, L929, and L02, respectively. The results indicate the excellent antitumor activity with good biocompatibility of AuNP@FeS4, which is ascribed to the released H_2S and the cascade activity.

Exploration of the Antitumor Mechanism *In Vitro*. The mechanism of the effective antitumor activity of AuNP@FeS4 in cancer cells was then investigated. Since the released H_2S from AuNP@FeS4 is expected to play a vital role in the antitumor process, we first monitored the intracellular H_2S level in 4T1 cells after incubation with AuNP@FeS4 by the WSP-1 probe.[45] Compared to PBS- or AuNP-treated cells, obvious green fluorescence, which indicates intracellular H_2S, is observed in FeSNP- or AuNP@FeS4-treated cells (Figure 4a). These results indicate that FeSNP and AuNP@FeS4 are endocytosed by cells and release H_2S, enhancing the intracellular H_2S level. In addition, AuNP@FeS4-treated cells present the highest intracellular H_2S level, as the highest green fluorescence is observed. These results are likely because Au nanozymes with GOD-like activity enhance acidity for promoting H_2S generation, which is consistent with the in vitro analysis of the H_2S releasing behavior of AuNP@FeS4. To further understand the intracellular H_2S release mechanism, the intracellular H_2S level and pH were explored by the WSP-1 probe and BCECF-AM after incubation with AuNP@FeS and 4T1 cells in DMEM containing different concentrations of glucose. AuNP@FeS presents a glucose-dependent H_2S release behavior, and more H_2S was released with the increased glucose concentration (Figure S7a). Meanwhile, BCECF-AM is a commercial pH fluorescence probe that can be clipped by intracellular esterase to form BCECF with a lower green fluorescence in an acidic environment.[46] The lower green fluorescence appears at higher glucose concentrations, indicating that the intracellular pH of AuNP@FeS4-treated cells presents glucose-dependent activity and becomes more acidic with the increased glucose concentration (Figure S7b). These results further indicate that AuNP in AuNP@FeS catalyzes glucose into gluconic acid and causes acidification, triggering released H_2S from AuNP@FeS, which induces enhanced acidity in tumor cells.

Considering the H_2S gas molecule can reduce H_2O_2 consumption by inhibiting CAT activity[47] and accelerate lactic acid generation,[48] the CAT expression in 4T1 cells was subsequently investigated with Western Blot (WB). Corresponding to the intracellular H_2S level, significantly inhibited CAT expression appears in FeSNP-treated cells and AuNP@FeS4-treated cells, and AuNP@FeS4 presents the highest CAT inhibition (Figure 4b). The CAT activity was further detected with the CAT assay kit, and the results verify AuNP@FeS4-treated cells show the highest CAT activity inhibition (Figure S8). These results demonstrate that the released H_2S from AuNP@FeS4 indeed inhibits CAT activity in tumor cells. As CAT has the function of consuming endogenous H_2O_2, the intracellular H_2O_2 level was detected with the H_2O_2 test kit (Figure 4c). Compared to PBS-treated cells, a significant increase in the intracellular H_2O_2 level appears in AuNP-treated cells due to the GOD-like activity of Au nanozymes, which can generate H_2O_2 in the process of catalyzing glucose. FeSNP-treated cells present a higher intracellular H_2O_2 level, which is caused by the released H_2S-induced CAT inhibition. Due to the synergistic effect of AuNP and H_2S, AuNP@FeS4-treated cells present the highest intracellular H_2O_2 level, which facilitates ROS generation of AuNP@FeS4. These results altogether confirm that AuNP@FeS4 can combine gas (H_2S) therapy to synergistically increase intracellular H_2O_2 concentration *via* opening the source (H_2O_2 self-supplied by Au nanozymes) and reducing the expenditure (CAT inhibition by H_2S).

Due to the capacity of H_2S for promoting lactic acid generation,[48] the intracellular lactic acid level was further explored with a lactic acid test kit (Figure 4d). The intracellular lactic acid level of FeSNP-treated or AuNP@FeS4-treated cells was significantly higher than that of AuNP-treated or PBS-treated cells, which could be ascribed to the H_2S-enhanced glucose uptake. Then, the intracellular pH level after different treatments was detected by using BCECF-AM[46] (Figure 4e). Compared to the PBS group, the intensity of green fluorescence obviously weakens in AuNP- and FeSNP-treated cells, indicating that gluconic acid generated by AuNP or lactic acid induced by H_2S can decrease the intracellular pH level. Due to the acidosis induced by the collaboration of

https://doi.org/10.1021/acsami.3c09066
ACS Appl. Mater. Interfaces 2023, 15, 46213−46225

generated gluconic acid and lactic acid, AuNP@FeS4-treated cells display the weakest green fluorescence, indicating the lowest intracellular pH level. This enhanced acid environment is supposed to be beneficial for ·OH generation by the FeS nanozyme with a POD-like activity or the Fenton reaction based on Fe^{2+} to induce ferroptosis in cancer cells.

Consequently, the intracellular ROS level was investigated with a DCFH-DA probe (Figure 4f). Although AuNP and FeSNP can both increase the intracellular H_2O_2 level and promote acidification to some extent, the high POD-like activity of FeSNP induces FeSNP-treated cells, presenting a higher ROS level than AuNP-treated cells as a significantly increased green fluorescence in FeSNP-treated cells is observed. AuNP@FeS4-treated cells present the strongest green fluorescence, indicating the highest intracellular ROS level, which is 23.94 and 7.47 times higher than that in AuNP- and FeSNP-treated cells, respectively, as a qualitative analysis *via* flow cytometry (Figure S9). These results firmly demonstrate that the boosted H_2O_2 and acidity synergistically induced by AuNP and H_2S can remarkably enhance •OH production efficiency by FeSNP in AuNP@FeS4. Meanwhile, the enhanced intracellular H_2O_2 level and acidification also facilitate ·OH generation by the released Fe^{2+}-mediated Fenton reaction, further enhancing the intracellular ROS level in AuNP@FeS4-treated cells.[44]

The accumulation of lipid peroxidation (LPO) is one of the hallmarks of ferroptosis,[3,49] which is reported to be abundantly expressed following the boosting ROS. Therefore, we next investigated the LPO expression in 4T1 cells by using the BODIPY-C11 probe, which presents excellent selectivity between oxidized (green fluorescence) and unoxidized lipid membranes (red fluorescence). The poor ROS generation of AuNP is insufficient for oxidizing lipid membranes, as a large amount of red fluorescence appears in AuNP-treated cells. However, the massive outbreaks of ROS induce AuNP@FeS4-treated cells to present a significant increase in LPO (green fluorescence, Figure 4g), which is higher than that of FeSNP-treated cells. In addition, the qualitative results of intracellular LPO level detection *via* flow cytometry indicate that AuNP@FeS4-treated cells present the highest intracellular LPO level (Figure S10). These results show that AuNP@FeS4 cascade nanozymes combining H_2S gas therapy with capacities of increasing H_2O_2 and acidosis can significantly amplify hallmarks of ferroptosis, *i.e.*, LPO, in tumor cells.

After the Fenton reaction, the generated Fe^{3+} can react with GSH to realize the recycling of Fe^{2+}, meanwhile expending GSH to inhibit GPX4 activity, which is an inhibitor of ferroptosis by protecting cells from LPO.[50] The down-regulation of GPX4 can be regarded as one of the hallmarks of ferroptosis. Thus, the GPX4 expression was detected by the WB method (Figure S11). Compared to PBS-, AuNP-, or FeSNP-treated cells, the GPX4 expression in AuNP@FeS4-treated cells is significantly suppressed. The GPX4 activity tested with an assay kit also showed that AuNP@FeS4-treated cells present the lowest GPX4 activity (Figure S12). These results indicate that AuNP@FeS4 also inhibits GPX4 activity to induce ferroptosis. After incubation with ferroptosis inhibitors, *i.e.*, ferrostatin-1 and *n*-acetyl cysteine (NAC), respectively, the decreases of cell viability induced by AuNP@FeS4 are significantly suppressed and present a concentration dependence (Figure S13). The cell viability can be recovered from 16.2 to 65.7% at 80 nM ferrostatin-1 and from 21.8 to 99.0% at 100 μM NAC, indicating it is indeed true that AuNP@FeS4 induces ferroptosis-mediated cell death in cancer cells. It is worth noting that the ferroptosis inhibition effect of NAC is better than that of fer-1, which may be due to their different mechanisms in ferroptosis inhibition. NAC not only directly eliminates radicals to inhibit LPO accumulation but also consumes LPO by providing GSH to increase the GPX4 activity.[51,52] However, fer-1 inhibits LPO formation,[53] which does not act directly on the upstream target of •OH accumulation. These results further show that the release of H_2S induces abundant generation of ROS, playing an important role in the ferroptosis therapy of AuNP@FeS4.

In addition, it is reported that the effects of H_2S on tumor proliferation and apoptosis were concentration-dependent. Low-concentration H_2S can promote tumor cell growth by upregulating antiapoptosis-related pathways or enhancing the antioxidant capacity, while high-concentration H_2S or low-concentration H_2S (20−200 μM) with a long exposure time inhibits tumor growth by inhibiting the NF-κB and signal transducer and activator of transcription 3 pathways to downregulate antiapoptotic proteins, inducing tumor cell apoptosis.[54−56] For example, the H_2S donor GYY4137 released low levels of H_2S (≤30 μM) for 5 d activated caspase activity, inducing cell apoptosis.[57] In our study, the concentration of released H_2S was relatively low (≤30 μM as shown in Figure 2i) and unlikely to induce apoptosis in tumor cells during a short period of culture (24 h). Thus, H_2S in this study mainly presents a synergistic effect to promote ferroptosis-mediated cancer cell death induced by AuNP@FeS.

All in all, the results demonstrate that AuNP@FeS4 kills tumor cells through H_2S-amplified ferroptosis. The Au nanozyme supplies H_2O_2 during the process of catalyzing glucose, and the released H_2S reduces H_2O_2 consumption by inhibiting CAT activity, thus cooperatively improving intracellular H_2O_2 accumulation. Meanwhile, the Au nanozyme can catalyze glucose into glucose acid, and the released H_2S can promote lactic acid conversion, inducing acidosis to enhance acidity in tumor cells. Altogether, the increasing intracellular H_2O_2 level and acidity facilitate FeS nanozymes with a POD-like activity and an Fe^{2+}-mediated Fenton reaction to boost •OH generation and then induce LPO accumulation and GPX4 inhibition, eventually achieving highly effective ferroptosis therapy.

In addition, we speculated that the CAT activity and released H_2S in normal cells are responsible for the good biocompatibility of AuNP@FeS4. This might have stemmed from the difference in pH values of the tumor and the normal tissue microenvironment. Due to the acid-responsive H_2S release behavior of AuNP@FeS4 (Figure 2l), the H_2S release might only occur in the acidic TME rather than in normal tissues with neutral pH. To verify this hypothesis, liver cells (L02 cells) presenting high CAT expression were chosen as the representative normal cells and the CAT activity was explored[58] (Figure S14). No obvious differences in CAT activity are observed in all four groups, indicating that CAT activity is not suppressed in L02 cells after treatment with AuNP@FeS4. This unaffected CAT activity can protect L02 cells from ferroptosis damage, maintaining an excellent cell viability. These results show the important role of H_2S in facilitating AuNP@FeS4, achieving effective antitumor bioactivity with good biocompatibility.

***In Vivo* Antitumor Activity of AuNP@FeS4.** Inspired by the encouraging results in vitro, we evaluated the in vivo antitumor activity of AuNP@FeS4 with 4T1 tumor-bearing

https://doi.org/10.1021/acsami.3c09066
ACS Appl. Mater. Interfaces 2023, 15, 46213−46225

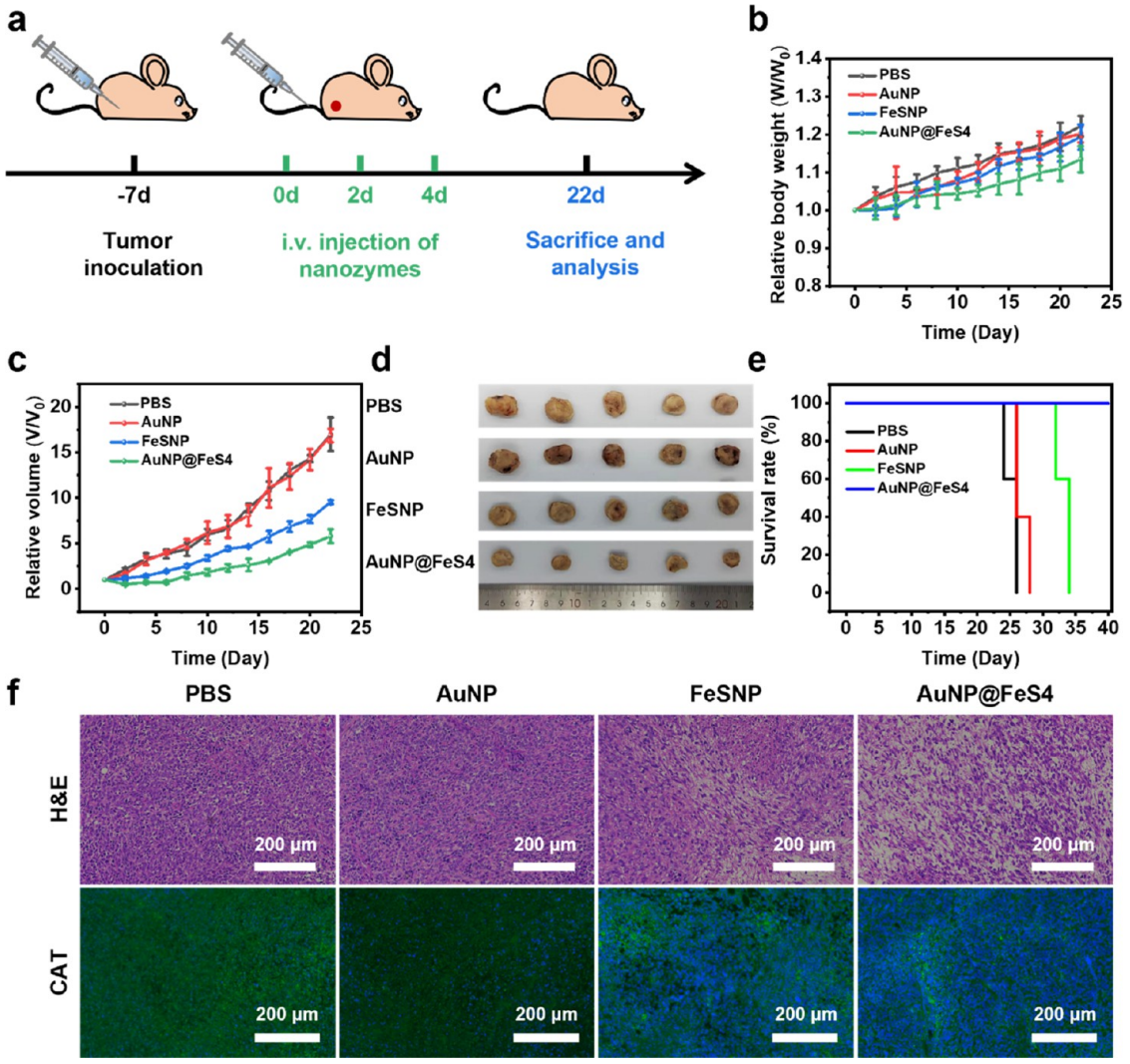

Figure 5. (a) Illustration of the therapeutic process *in vivo*. (b, c) Relative body weight (b) and tumor volume (c) of 4T1 tumor-bearing mice treated with PBS, AuNP, FeSNP, or AuNP@FeS4. (d) Representative tumor photograph after being treated with PBS, AuNP, FeSNP, or AuNP@FeS4 on 22 d post therapy. (e) Survival rate cures of mice after being treated with PBS, AuNP, FeSNP, or AuNP@FeS4. (f) H&E staining and CAT immunofluorescence images of tumor slices after being treated with PBS, AuNP, FeSNP, or AuNP@FeS4 on 22 d post therapy. The CAT expressions were labeled green, and the nuclei were labeled blue.

BALB/c mice (Figure 5a). After intravenous injection at 0, 2, and 4 d, the therapeutic process was monitored for 22 d. The relative body weights of mice were analyzed and are shown in Figure 5b. Increased steadily relative body weights are observed in all of the nanozymes during this period, showing the good biosafety of these nanozymes. Meanwhile, the relative tumor volumes were measured to evaluate the tumor therapeutic effect (Figure 5c). AuNP shows little tumor suppression effect as the tumor growth trend is similar to that in the PBS group. Compared to AuNP and PBS groups, the tumor growth tendency in the FeSNP group is significantly inhibited, indicating the good tumor suppression of FeSNP. It is also observed that AuNP@FeS4 presents the best tumor inhibition effect among all of the nanozymes with a tumor growth inhibition rate of 65.8%, which is ascribed to the synergistic effect between released H_2S and the cascade activity caused by the GOD-like activity and POD-like activity. The released H_2S can inhibit CAT activity and promote acidification, amplifying the therapeutic effect of ferroptosis. The digital images of tumors in each group also show the highest therapeutic effect of AuNP@FeS4 during the therapy period (Figure 5d). In addition, the survival rate was calculated (Figure 5e). The mice start to die at 24 and 26 d and are all dead at 26 and 28 d in PBS or the AuNP group after therapy. After 32 days of therapy, the survival rates of PBS, AuNP, FeSNP, and AuNP@FeS4 groups were 0.0, 0.0, 60.0, and 100%, respectively. Surprisingly, the AuNP@FeS4 group maintains a 100% survival rate even at 40 days post treatment, indicating an excellent tumor inhibition effect.

Then, H&E stainings were used to analyze the pathological changes of the tumor tissues on all of the nanozymes at 22 d (Figure 5f). Compared to PBS and AuNP groups, the loose intercellular space and reduced tumor cells are clearly observed in the FeSNP group, indicating that FeSNP can induce tumor cell death. AuNP@FeS4 shows the most serious tumor cell damage as abundant loose intercellular space and reduced tumor cells appear. To explore the cytotoxic mechanism of AuNP@FeS4 in tumor tissues, immunohistochemical analysis of CAT and GPX4 was carried out, and the expression was labeled as green fluorescence (Figures 5f and S15). Due to the

https://doi.org/10.1021/acsami.3c09066
ACS Appl. Mater. Interfaces 2023, 15, 46213−46225

released H_2S, the CAT expression is significantly inhibited in FeSNP and AuNP@FeS4 groups, and the latter is the lowest in all groups. Moreover, the GPX4 expression level corresponds to the CAT expression and AuNP@FeS4 displays the highest ferroptosis ability as the GPX4 expression level is the lowest. These results further prove that CAT inhibition has a positive correlation to ferroptosis in tumor tissues, and the ferroptosis therapy of AuNP@FeS4 is amplified by the released H_2S, inducing excellent tumor therapeutic effects *in vivo*.

***In Vivo* Biocompatibility Evaluation.** *In vivo* biosafety and biocompatibility evaluation of AuNP@FeS4 is greatly significant to further promote clinical translation. The hemocompatibility was evaluated by a hemolysis assay (Figure S16). After incubation with red blood cells of mice, the hemolysis rate of the AuNP@FeS4 group is still below 5.0% with the high dose (at the Fe concentration of 100 μg/mL), indicating that AuNP@FeS4 exhibits a high hemocompatibility. Then, the pharmacokinetics and *in vivo* distribution were evaluated by monitoring the Fe concentration in the blood, major organs (heart, liver, spleen, lung, and kidney), and tumor after intravenous injection *via* inductively coupled plasma-optical emission spectrometry (ICP-OES) (Figures S17 and S18). Fe% ID/g in plasma decreases sharply in a short time, and AuNP@FeS4 shows a blood circulation half-time of 2.11 h. Meanwhile, AuNP@FeS4 is mainly distributed in the spleen, liver, kidneys, and tumor. The Fe content in the liver and kidney decreases with time, which is mainly due to metabolism and excretion. AuNP@FeS4 enriches rapidly at 3 h after intravenous injection, reaches the highest level at 6 h, which is as high as 34.08% ID/g, and still exists in tumor tissues at 24 h. This high tumor uptake and prolonged retention are benefits of tumor therapy. The standard hematology analysis was performed to evaluate the potential risk of nanomaterials inducing inflammatory responses. After intravenous injection with AuNP@FeS4 at the dosages of 5, 10, and 15 mg/mL for 7 d, the red blood cell count and biochemical indexes showed no significant changes compared to that of PBS (Table S3). Meanwhile, there are no significant differences in the blood levels, such as alanine transaminase (ALT), aspartate transaminase (AST), blood urea nitrogen (BUN), creatinine (CR), and creatine kinase (CK, Figure S19). These data indicate that AuNP@FeS4 has no significant toxicity to the liver and kidney. No obvious damage is observed in the histological morphology of the major organs,[59] which further indicates that AuNP@FeS4 presents good biological safety during the therapy period (Figure S20). These results indicate that AuNP@FeS4 can significantly inhibit tumor growth and effectively prolong the life span of mice, providing important guidance for further clinical translation of the developed AuNP@FeS4.

Both *in vitro* and *in vivo* studies indicate the excellent ability of ferroptosis induction by AuNP@FeS to kill tumor cells. First, the insufficient H_2O_2 and acidity in the TME are significant challenges for ferroptosis-based tumor therapy in the field of nanozymes. Compared to case platform and gas therapy, the combination of case nanozymes and gas therapy molecule H_2S provides an effective strategy to improve the accumulation of H_2O_2 and acidity in the TME, which promotes nanozymes to generate abundant $^{\bullet}OH$ for inducing ferroptosis. Second, particle size is an important factor that affects nanozyme catalytic activity. For example, Zhang et al. designed a single-atom nanozyme (SAzyme) with an atomically dispersed Cu−N4 site, exhibiting a superior superoxide dismutase-like activity.[60] In this study, the ultrasmall size also enables AuNP@FeS to efficiently catalyze the transformation of H_2O_2 into $^{\bullet}OH$ for tumor therapy. Third, the H_2S-amplified ferroptosis mechanism makes AuNP@FeS present excellent tumor inhibition performance with good biocompatibility, which is conducive to realizing safe tumor therapy. In addition, the bioactive protein molecule BSA also contributes to the good biocompatibility.[29,30] These features make AuNP@FeS display a huge prospect in the clinical translation for tumor therapy, especially for drug-resistant tumors as ferroptosis can kill drug-resistant tumor cells.[4] However, some important issues still need to be resolved before clinical applications. For example, further follow-up studies are required to improve the tumor targeting as well as immune escape ability of AuNP@FeS,[61,62] such as surface modification of RGD peptides or polymers like PEG.[63−65] In addition, the intertumoral distribution and increased safety trials, such as immunogenicity, immunotoxicity, and long-term toxicity analysis, need to be tested for further clinical translation.[66]

CONCLUSIONS

In summary, we have developed a H_2S-releasing ultrasmall cascade nanozyme AuNP@FeS4 to increase H_2O_2 concentration and acidity in tumor cells for promoting $^{\bullet}OH$ generation, achieving gas-amplified ferroptosis. The ultrasmall size makes AuNP@FeS4 exhibit high cascade activity based on GOD-like and POD-like activity. Meanwhile, AuNP@FeS4 displays an acid-response cascade activity and a H_2S release behavior. Due to the GOD-like activity of the Au nanozyme, AuNP@FeS4 self-supplies H_2O_2 by catalyzing glucose for the FeS nanozyme with POD-like activity to generate $^{\bullet}OH$, inducing ferroptosis. Then, released H_2S significantly inhibits the CAT activity in tumor cells and decreases H_2O_2 consumption, further increasing the intracellular H_2O_2 level. Since gluconic acid is also generated when the Au nanozyme catalyzes glucose, accompanied by the lactic acid conversion by released H_2S, AuNP@FeS4 induces acidosis to further improve the acidity and accelerate $^{\bullet}OH$ generation, achieving high tumor therapeutic effects through H_2S-amplified ferroptosis. In normal cells, AuNP@FeS4 exhibits good biocompatibility, as CAT activity is not inhibited. *In vivo* data further prove that the H_2S-amplified ferroptosis makes AuNP@FeS4 display excellent tumor therapeutic effects. Moreover, AuNP@FeS4 shows no biotoxicity to major organs, indicating its high biocompatibility. The AuNP@FeS4 cascade nanozyme causes highly effective tumor therapy through H_2S amplified ferroptosis, showing great promise in further clinical translation applications and paving the way in the development of a gas-amplified ferroptosis therapeutic system based on nanozymes for tumor therapy.

ASSOCIATED CONTENT

Supporting Information

The Supporting Information is available free of charge at https://pubs.acs.org/doi/10.1021/acsami.3c09066.

Experimental section; characterization data including TEM morphology; XPS survey spectrum; ζ-potential; antitumor activity and antitumor mechanism data including cell viability, CAT activity, intracellular ROS fluorescence distributions, intracellular LPO fluorescence distributions, *in vitro* or *in vivo* GPX4 expression; and *in vivo* biocompatibility data including hemolysis, pharmacokinetics, blood routine analysis, biochemical

https://doi.org/10.1021/acsami.3c09066
ACS Appl. Mater. Interfaces 2023, 15, 46213−46225

analysis, and H&E staining images of major organs (PDF)

AUTHOR INFORMATION

Corresponding Authors

Sugeun Yang − *Department of Biomedical Science, BK21 FOUR Program in Biomedical Science and Engineering, Inha University College of Medicine, Incheon 22212, South Korea*; Email: sugeun.yang@inha.ac.kr

Zheyu Shen − *School of Biomedical Engineering, Southern Medical University, Guangzhou, Guangdong 510515, China*; orcid.org/0000-0002-0350-375X; Email: sz@smu.edu.cn

Authors

Jiezhao Zhan − *School of Biomedical Engineering, Southern Medical University, Guangzhou, Guangdong 510515, China*

Jianping Liu − *School of Biomedical Engineering, Southern Medical University, Guangzhou, Guangdong 510515, China*

Jing Yang − *School of Biomedical Engineering, Southern Medical University, Guangzhou, Guangdong 510515, China*

Lin Huang − *School of Biomedical Engineering, Southern Medical University, Guangzhou, Guangdong 510515, China*

Yudie Lu − *School of Biomedical Engineering, Southern Medical University, Guangzhou, Guangdong 510515, China*

Xuanyi Lu − *School of Biomedical Engineering, Southern Medical University, Guangzhou, Guangdong 510515, China*

Jiaoyang Zhu − *School of Biomedical Engineering, Southern Medical University, Guangzhou, Guangdong 510515, China*

Complete contact information is available at: https://pubs.acs.org/10.1021/acsami.3c09066

Notes

The authors declare no competing financial interest.

ACKNOWLEDGMENTS

This work was financially supported by the China Postdoctoral Foundation Project (2022M711529), the Guangdong Provincial Natural Science Foundation of China (2021A1515010605), the National Natural Science Foundation of China (32271374), and the Guangzhou Key Research and Development Program of China (202103000094). All animal procedures were performed under the Guidelines for Care and Use of Laboratory Animals of Southern Medical University and approved by the Animal Ethics Committee of Southern Medical University. The assigned approval/accreditation number is SYXK(YUE)2021-0167.

REFERENCES

(1) Guo, X.; Liu, F.; Deng, J.; Dai, P.; Qin, Y.; Li, Z.; Wang, B.; Fan, A.; Wang, Z.; Zhao, Y. Electron-Accepting Micelles Deplete Reduced Nicotinamide Adenine Dinucleotide Phosphate and Impair Two Antioxidant Cascades for Ferroptosis-Induced Tumor Eradication. *ACS Nano* **2020**, *14* (11), 14715−14730.

(2) Lei, G.; Zhuang, L.; Gan, B. Targeting ferroptosis as a vulnerability in cancer. *Nat. Rev. Cancer* **2022**, *22* (7), 381−396.

(3) Guo, S.; Li, Z.; Feng, J.; Xiong, W.; Yang, J.; Lu, X.; Yang, S.; Xu, Y.; Wu, A.; Shen, Z. Cycloacceleration of ferroptosis and calcicoptosis for magnetic resonance imaging-guided colorectal cancer therapy. *Nano Today* **2022**, *47*, No. 101663.

(4) Yue, R.; Zhang, C.; Xu, L.; Wang, Y.; Guan, G.; Lei, L.; Zhang, X.; Song, G. Dual key co-activated nanoplatform for switchable MRI monitoring accurate ferroptosis-based synergistic therapy. *Chem* **2022**, *8* (7), 1956−1981.

(5) Chang, M.; Hou, Z.; Wang, M.; Yang, C.; Wang, R.; Li, F.; Liu, D.; Peng, T.; Li, C.; Lin, J. Single-atom Pd nanozyme for ferroptosis-boosted mild-temperature photothermal therapy. *Angew. Chem., Int. Ed.* **2021**, *60* (23), 12971−12979.

(6) Zhong, Y.; Zhang, J.; Zhang, J.; Hou, Y.; Chen, E.; Huang, D.; Chen, W.; Haag, R. Tumor Microenvironment-Activatable Nanoenzymes for Mechanical Remodeling of Extracellular Matrix and Enhanced Tumor Chemotherapy. *Adv. Funct. Mater.* **2021**, *31* (3), No. 2007544.

(7) Zeng, W.; Yu, M.; Chen, T.; Liu, Y.; Yi, Y.; Huang, C.; Tang, J.; Li, H.; Ou, M.; Wang, T.; Wu, M.; Mei, L. Polypyrrole Nanoenzymes as Tumor Microenvironment Modulators to Reprogram Macrophage and Potentiate Immunotherapy. *Adv. Sci.* **2022**, *9* (23), No. 2201703.

(8) Tao, N.; Li, H.; Deng, L.; Zhao, S.; Ouyang, J.; Wen, M.; Chen, W.; Zeng, K.; Wei, C.; Liu, Y.-N. A Cascade Nanozyme with Amplified Sonodynamic Therapeutic Effects through Comodulation of Hypoxia and Immunosuppression against Cancer. *ACS Nano* **2022**, *16* (1), 485−501.

(9) Chen, X.; Zhang, H.; Zhang, M.; Zhao, P.; Song, R.; Gong, T.; Liu, Y.; He, X.; Zhao, K.; Bu, W. Amorphous Fe-Based Nanoagents for Self-Enhanced Chemodynamic Therapy by Re-Establishing Tumor Acidosis. *Adv. Funct. Mater.* **2019**, *30* (6), No. 1908365, DOI: 10.1002/adfm.201908365.

(10) Zhu, X.; Wu, J.; Liu, R.; Xiang, H.; Zhang, W.; Chang, Q.; Wang, S.; Jiang, R.; Zhao, F.; Li, Q.; et al. Engineering Single-Atom Iron Nanozymes with Radiation-Enhanced Self-Cascade Catalysis and Self-Supplied H2O2 for Radio-enzymatic Therapy. *ACS Nano* **2022**, *16* (11), 18849−18862.

(11) Li, L.; Yang, Z.; Fan, W.; He, L.; Cui, C.; Zou, J.; Tang, W.; Jacobson, O.; Wang, Z.; Niu, G.; et al. In situ polymerized hollow mesoporous organosilica biocatalysis nanoreactor for enhancing ROS-mediated anticancer therapy. *Adv. Funct. Mater.* **2020**, *30* (4), No. 1907716.

(12) Peng, M.; Ju, E.; Xu, Y.; Wang, Y.; Lv, S.; Shao, D.; Wang, H.; Tao, Y.; Zheng, Y.; Li, M. Dual-responsive disassembly of core-shell nanoparticles with self-supplied H2O2 and autocatalytic Fenton reaction for enhanced chemodynamic therapy. *NPG Asia Mater.* **2022**, *14* (1), No. 95.

(13) Chen, J.; Liu, X.; Zheng, G.; Feng, W.; Wang, P.; Gao, J.; Liu, J.; Wang, M.; Wang, Q. Detection of Glucose Based on Noble Metal Nanozymes: Mechanism, Activity Regulation, and Enantioselective Recognition. *Small* **2022**, *19*, No. 2205924, DOI: 10.1002/smll.202205924.

(14) Gao, S. S.; Lin, H.; Zhang, H. X.; Yao, H. L.; Chen, Y.; Shi, J. L. Nanocatalytic Tumor Therapy by Biomimetic Dual Inorganic Nanozyme-Catalyzed Cascade Reaction. *Adv. Sci.* **2019**, *6* (3), No. 1801733.

(15) Sun, K.; Hu, J.; Meng, X.; Lei, Y.; Zhang, X.; Lu, Z.; Zhang, L.; Wang, Z. Reinforcing the Induction of Immunogenic Cell Death Via Artificial Engineered Cascade Bioreactor-Enhanced Chemo-Immunotherapy for Optimizing Cancer Immunotherapy. *Small* **2021**, *17* (37), No. 2101897.

(16) Martínez-Reyes, I.; Chandel, N. S. Cancer metabolism: looking forward. *Nat. Rev. Cancer* **2021**, *21* (10), 669−680.

(17) Gong, F.; Chen, M.; Yang, N.; Dong, Z.; Tian, L.; Hao, Y.; Zhuo, M.; Liu, Z.; Chen, Q.; Cheng, L. Bimetallic Oxide FeWOX Nanosheets as Multifunctional Cascade Bioreactors for Tumor Microenvironment-Modulation and Enhanced Multimodal Cancer Therapy. *Adv. Funct. Mater.* **2020**, *30* (49), No. 2002753.

(18) Reinfeld, B. I.; Madden, M. Z.; Wolf, M. M.; Chytil, A.; Bader, J. E.; Patterson, A. R.; Sugiura, A.; Cohen, A. S.; Ali, A.; Do, B. T.; Muir, A.; Lewis, C. A.; Hongo, R. A.; Young, K. L.; Brown, R. E.; Todd, V. M.; Huffstater, T.; Abraham, A.; O'Neil, R. T.; Wilson, M. H.; Xin, F.; Tantawy, M. N.; Merryman, W. D.; Johnson, R. W.; Williams, C. S.; Mason, E. F.; Mason, F. M.; Beckermann, K. E.; Vander Heiden, M. G.; Manning, H. C.; Rathmell, J. C.; Rathmell, W. K. Cell-programmed nutrient partitioning in the tumour microenvironment. *Nature* **2021**, *593* (7858), 282−288.

(19) Lu, J. The Warburg metabolism fuels tumor metastasis. *Cancer Metastasis Rev.* **2019**, *38* (1), 157−164.
(20) Rong, F.; Wang, T.; Zhou, Q.; Peng, H.; Yang, J.; Fan, Q.; Li, P. Intelligent polymeric hydrogen sulfide delivery systems for therapeutic applications. *Bioact. Mater.* **2023**, *19*, 198−216.
(21) Chen, L.; Zhou, S.-F.; Su, L.; Song, J. Gas-Mediated Cancer Bioimaging and Therapy. *ACS Nano* **2019**, *13* (10), 10887−10917.
(22) Fang, C.; Cen, D.; Wang, Y.; Wu, Y.; Cai, X.; Li, X.; Han, G. ZnS@ZIF-8 core-shell nanoparticles incorporated with ICG and TPZ to enable H(2)S-amplified synergistic therapy. *Theranostics* **2020**, *10* (17), 7671−7682.
(23) Cen, D.; Ge, Q.; Xie, C.; Zheng, Q.; Guo, J.; Zhang, Y.; Wang, Y.; Li, X.; Gu, Z.; Cai, X. ZnS@BSA Nanoclusters Potentiate Efficacy of Cancer Immunotherapy. *Adv. Mater.* **2021**, *33* (49), No. e2104037.
(24) Wan, M.; Liu, Z.; Li, T.; Chen, H.; Wang, Q.; Chen, T.; Tao, Y.; Mao, C. Zwitterion-Based Hydrogen Sulfide Nanomotors Induce Multiple Acidosis in Tumor Cells by Destroying Tumor Metabolic Symbiosis. *Angew. Chem., Int. Ed.* **2021**, *60* (29), 16139−16148.
(25) Xie, C.; Cen, D.; Ren, Z.; Wang, Y.; Wu, Y.; Li, X.; Han, G.; Cai, X. FeS@ BSA nanoclusters to enable H2S-amplified ROS-based therapy with MRI guidance. *Adv. Sci.* **2020**, *7* (7), No. 1903512.
(26) Wang, J.; Sun, Z.; Wang, S.; Zhao, C.; Xu, J.; Gao, S.; Yang, M.; Sheng, F.; Gao, S.; Hou, Y. Biodegradable Ferrous Sulfide-Based Nanocomposites for Tumor Theranostics through Specific Intratumoral Acidosis-Induced Metabolic Symbiosis Disruption. *J. Am. Chem. Soc.* **2022**, *144* (43), 19884−19895.
(27) Ai, Y.; Hu, Z.-N.; Liang, X.; Sun, H.-b.; Xin, H.; Liang, Q. Recent Advances in Nanozymes: From Matters to Bioapplications. *Adv. Funct. Mater.* **2022**, *32* (14), No. 2110432.
(28) Chen, J.; Liu, X.; Zheng, G.; Feng, W.; Wang, P.; Gao, J.; Liu, J.; Wang, M.; Wang, Q. Detection of Glucose Based on Noble Metal Nanozymes: Mechanism, Activity Regulation, and Enantioselective Recognition. *Small* **2023**, *19* (8), No. 2205924.
(29) Tian, Q.; Li, Y.; Jiang, S.; An, L.; Lin, J.; Wu, H.; Huang, P.; Yang, S. Tumor pH-Responsive Albumin/Polyaniline Assemblies for Amplified Photoacoustic Imaging and Augmented Photothermal Therapy. *Small* **2019**, *15* (42), No. 1902926.
(30) Ou, J.; Liu, K.; Jiang, J.; Wilson, D. A.; Liu, L.; Wang, F.; Wang, S.; Tu, Y.; Peng, F. Micro-/Nanomotors toward Biomedical Applications: The Recent Progress in Biocompatibility. *Small* **2020**, *16* (27), No. 1906184.
(31) Petrella, L.; Thébaud, N.; Fougerouse, D.; Tattitch, B.; Martin, L.; Turner, S.; Suvorova, A.; Gain, S. Nanoparticle suspensions from carbon-rich fluid make high-grade gold deposits. *Nat. Commun.* **2022**, *13* (1), No. 3795.
(32) Young, A. J.; Sauer, M.; Rubio, G. M.; Sato, A.; Foelske, A.; Serpell, C. J.; Chin, J. M.; Reithofer, M. R. One-step synthesis and XPS investigations of chiral NHC−Au (0)/Au (I) nanoparticles. *Nanoscale* **2019**, *11* (17), 8327−8333.
(33) Yang, D.; Chen, W.; Zhang, X.; Mi, L.; Liu, C.; Chen, L.; Guan, X.; Cao, Y.; Shen, C. Facile and scalable synthesis of low-cost FeS@ C as long-cycle anodes for sodium-ion batteries. *J. Mater. Chem. A* **2019**, *7* (34), 19709−19718.
(34) Yang, W.; Xiang, C.; Xu, Y.; Chen, S.; Zeng, W.; Liu, K.; Jin, X.; Zhou, X.; Zhang, B. Albumin-constrained large-scale synthesis of renal clearable ferrous sulfide quantum dots for T1-Weighted MR imaging and phototheranostics of tumors. *Biomaterials* **2020**, *255*, No. 120186.
(35) Le Guével, X.; Hötzer, B.; Jung, G.; Hollemeyer, K.; Trouillet, V.; Schneider, M. Formation of Fluorescent Metal (Au, Ag) Nanoclusters Capped in Bovine Serum Albumin Followed by Fluorescence and Spectroscopy. *J. Phys. Chem. C* **2011**, *115* (22), 10955−10963.
(36) Meng, X.; Li, D.; Chen, L.; He, H.; Wang, Q.; Hong, C.; He, J.; Gao, X.; Yang, Y.; Jiang, B. High-performance self-cascade pyrite nanozymes for apoptosis−ferroptosis synergistic tumor therapy. *ACS Nano* **2021**, *15* (3), 5735−5751, DOI: 10.1021/acsnano.1c01248.
(37) Comotti, M.; Pina, C. D.; Matarrese, R.; Rossi, M. The Catalytic Activity of "Naked" Gold Particles. *Angew. Chem., Int. Ed.* **2004**, *43* (43), 5812−5815, DOI: 10.1002/anie.200460446.
(38) Liu, B.; Liu, J. Surface modification of nanozymes. *Nano Res.* **2017**, *10* (4), 1125−1148.
(39) Zhang, H.; Liang, X.; Han, L.; Li, F. Non-Naked" Gold with Glucose Oxidase-Like Activity: A Nanozyme for Tandem Catalysis. *Small* **2018**, *14* (44), No. 1803256, DOI: 10.1002/smll.201803256.
(40) You, C.; Li, X.; Wang, D.; Chen, H.; Liang, L.; Chen, Y.; Zhao, Y.; Xiang, H. Self-Assembled Aza-Boron-Dipyrromethene for Ferroptosis-Boosted Sonodynamic Therapy. *Angew. Chem., Int. Ed.* **2022**, *61* (41), No. e202210174, DOI: 10.1002/anie.202210174.
(41) Wang, P.; Liu, S.; Hu, M.; Zhang, H.; Duan, D.; He, J.; Hong, J.; Lv, R.; Choi, H. S.; Yan, X.; Liang, M. Peroxidase-Like Nanozymes Induce a Novel Form of Cell Death and Inhibit Tumor Growth In Vivo. *Adv. Funct. Mater.* **2020**, *30* (21), No. 2000647.
(42) Lin, J.; Li, Y.; Wang, P.; Wu, M.; Zhu, F.; Zhang, Y.; Hou, Z.; Liu, J.; Liu, X. Natural Killer Cell Membrane-Cloaked Virus-Mimicking Nanogenerator with NIR-Triggered Shape Reversal and •C/•OH Storm for Synergistic Thermodynamic−Chemodynamic Therapy. *Adv. Sci.* **2022**, *9* (5), No. 2103498, DOI: 10.1002/advs.202103498.
(43) Wu, Z.; Zhang, Y.; Zhang, L.; Zhou, B.; Wei, Z.; Wang, D.; Lu, W.; Jia, J.; Tao, L.; Wang, T.; Wang, S. Coupling Fe(II)/Fe(III) Redox Mediated SO_2 Conversion with Hydrogen Production. *Adv. Funct. Mater.* **2023**, *33* (10), No. 2212479.
(44) Jiang, Z.; Wang, L.; Lei, J.; Liu, Y.; Zhang, J. Photo-Fenton Degradation of Phenol by CdS/rGO/Fe2+ at Natural pH with in Situ-Generated H_2O_2. *Appl. Catal., B* **2019**, *241*, 367−374.
(45) Li, G.; Lei, H.; Yang, Y.; Zhong, X.; Gong, F.; Gong, Y.; Zhou, Y.; Zhang, Y.; Shi, H.; Xiao, Z. Titanium Sulfide Nanosheets Serve as Cascade Bioreactors for H_2S-Mediated Programmed Gas−Sonodynamic Cancer Therapy. *Adv. Sci.* **2022**, *9* (30), No. 2201069, DOI: 10.1002/advs.202201069.
(46) Li, W.; Yin, S.; Shen, Y.; Li, H.; Yuan, L.; Zhang, X.-B. Molecular Engineering of pH-Responsive NIR Oxazine Assemblies for Evoking Tumor Ferroptosis via Triggering Lysosomal Dysfunction. *J. Am. Chem. Soc.* **2023**, *145* (6), 3736−3747.
(47) Sang, Y.; Cao, F.; Li, W.; Zhang, L.; You, Y.; Deng, Q.; Dong, K.; Ren, J.; Qu, X. Bioinspired Construction of a Nanozyme-Based H_2O_2 Homeostasis Disruptor for Intensive Chemodynamic Therapy. *J. Am. Chem. Soc.* **2020**, *142* (11), 5177−5183.
(48) Wang, Y.; Qian, M.; Du, Y.; Zhou, J.; Huo, T.; Guo, W.; Akhtar, M.; Huang, R. Tumor-Selective Biodegradation-Regulated Photothermal H2S Donor for Redox Dyshomeostasis-and Glycolysis Disorder-Enhanced Theranostics. *Small* **2022**, *18* (8), No. 2106168.
(49) Huang, L.; Lu, Y.; Guo, S.; Yang, J.; Liang, Z.; Zhang, Q.; Yi, P.; Feng, Y.; Li, Y.; Xu, Y.; et al. A Strategy of Limited-Space Controlled Aggregation for Generic Enhancement of Drug Loading Capability. *Adv. Funct. Mater.* **2023**, *33* (4), No. 2209278.
(50) Li, P.; Jiang, M.; Li, K.; Li, H.; Zhou, Y.; Xiao, X.; Xu, Y.; Krishfield, S.; Lipsky, P. E.; Tsokos, G. C.; Zhang, X. Glutathione Peroxidase 4−Regulated Neutrophil Ferroptosis Induces Systemic Autoimmunity. *Nat. Immunol.* **2021**, *22* (9), 1107−1117.
(51) Mlejnek, P. Direct Interaction between N-Acetylcysteine and Cytotoxic Electrophile—An Overlooked In Vitro Mechanism of Protection. *Antioxidants* **2022**, *11* (8), No. 1485, DOI: 10.3390/antiox11081485.
(52) Guo, J.; Duan, L.; He, X.; Li, S.; Wu, Y.; Xiang, G.; Bao, F.; Yang, L.; Shi, H.; Gao, M.; Zheng, L.; Hu, H.; Liu, X. A Combined Model of Human iPSC-Derived Liver Organoids and Hepatocytes Reveals Ferroptosis in DGUOK Mutant mtDNA Depletion Syndrome. *Adv. Sci.* **2021**, *8* (10), No. 2004680.
(53) Miotto, G.; Rossetto, M.; Di Paolo, M. L.; Orian, L.; Venerando, R.; Roveri, A.; Vučković, A.-M.; Travain, V. B.; Zaccarin, M.; Zennaro, L.; Maiorino, M.; Toppo, S.; Ursini, F.; Cozza, G. Insight into the Mechanism of Ferroptosis Inhibition by Ferrostatin-1. *Redox Biol.* **2020**, *28*, No. 101328, DOI: 10.1016/j.redox.2019.101328.
(54) Hu, X.; Xiao, Y.; Sun, J.; Ji, B.; Luo, S.; Wu, B.; Zheng, C.; Wang, P.; Xu, F.; Cheng, K.; Hua, H.; Li, D. New Possible Silver

Lining for Pancreatic Cancer Therapy: Hydrogen Sulfide and Its Donors. *Acta Pharm. Sin. B* **2021**, *11* (5), 1148−1157.
(55) Kashfi, K. Anti-Cancer Activity of New Designer Hydrogen Sulfide-Donating Hybrids. *Antioxid. Redox Signaling* **2014**, *20* (5), 831−846, DOI: 10.1089/ars.2013.5308.
(56) Lu, S.; Gao, Y.; Huang, X.; Wang, X. GYY4137, a Hydrogen Sulfide (H_2S) donor, Shows Potent Anti-Hepatocellular Carcinoma Activity through Blocking the STAT3 Pathway. *Int. J. Oncol.* **2014**, *44* (4), 1259−1267.
(57) Lee, Z. W.; Zhou, J.; Chen, C.-S.; Zhao, Y.; Tan, C.-H.; Li, L.; Moore, P. K.; Deng, L.-W. The Slow-Releasing Hydrogen Sulfide Donor, GYY4137, Exhibits Novel Anti-Cancer Effects In Vitro and In Vivo. *PLoS One* **2011**, *6* (6), No. e21077.
(58) Rakic, J. M.; Liu, C.; Veeramachaneni, S.; Wu, D.; Paul, L.; Ausman, L. M.; Wang, X.-D. Dietary Lycopene Attenuates Cigarette Smoke-Promoted Nonalcoholic Steatohepatitis by Preventing Suppression of Antioxidant Enzymes in Ferrets. *J. Nutr. Biochem.* **2021**, *91*, No. 108596, DOI: 10.1016/j.jnutbio.2021.108596.
(59) Lu, Y.; Feng, J.; Liang, Z.; Lu, X.; Guo, S.; Huang, L.; Xiong, W.; Chen, S.; Zhou, H.; Ma, X.; et al. A Tumor Microenvironment Dual Responsive Contrast agent for Contrary Contrast-Magnetic Resonance Imaging and Specific Chemotherapy of Tumors. *Nanoscale Horiz.* **2022**, *7* (4), 403−413.
(60) Yang, J.; Zhang, R.; Zhao, H.; Qi, H.; Li, J.; Li, J.-F.; Zhou, X.; Wang, A.; Fan, K.; Yan, X.; Zhang, T. Bioinspired Copper Single-Atom Nanozyme as a Superoxide Dismutase-Like Antioxidant for Sepsis Treatment. *Exploration* **2022**, *2* (4), No. 20210267.
(61) Zeng, Z.; Pu, K. Improving Cancer Immunotherapy by Cell Membrane-Camouflaged Nanoparticles. *Adv. Funct. Mater.* **2020**, *30* (43), No. 2004397.
(62) Li, B.; Chu, T.; Wei, J.; Zhang, Y.; Qi, F.; Lu, Z.; Gao, C.; Zhang, T.; Jiang, E.; Xu, J.; Xu, J.; Li, S.; Nie, G. Platelet-Membrane-Coated Nanoparticles Enable Vascular Disrupting Agent Combining Anti-Angiogenic Drug for Improved Tumor Vessel Impairment. *Nano Lett.* **2021**, *21* (6), 2588−2595.
(63) Zang, J.; Wen, X.; Lin, R.; Zeng, X.; Wang, C.; Shi, M.; Zeng, X.; Zhang, J.; Wu, X.; Zhang, X.; Miao, W.; Xu, P.; Guo, Z.; Zhang, J.; Chen, X. Synthesis, Preclinical Evaluation and Radiation Dosimetry of a Dual Targeting PET tracer [(68)Ga]Ga-FAPI-RGD. *Theranostics* **2022**, *12* (16), 7180−7190.
(64) Hu, X.; Wang, N.; Guo, X.; Liang, Z.; Sun, H.; Liao, H.; Xia, F.; Guan, Y.; Lee, J.; Ling, D.; Li, F. A Sub-Nanostructural Transformable Nanozyme for Tumor Photocatalytic Therapy. *Nano-Micro Lett.* **2022**, *14* (1), No. 101, DOI: 10.1007/s40820-022-00848-y.
(65) Sacchetti, C.; Motamedchaboki, K.; Magrini, A.; Palmieri, G.; Mattei, M.; Bernardini, S.; Rosato, N.; Bottini, N.; Bottini, M. Surface Polyethylene Glycol Conformation Influences the Protein Corona of Polyethylene Glycol-Modified Single-Walled Carbon Nanotubes: Potential Implications on Biological Performance. *ACS Nano* **2013**, *7* (3), 1974−1989.
(66) Ang, M. J. Y.; Chan, S. Y.; Goh, Y.-Y.; Luo, Z.; Lau, J. W.; Liu, X. Emerging Strategies in Developing Multifunctional Nanomaterials for Cancer Nanotheranostics. *Adv. Drug Delivery Rev.* **2021**, *178*, No. 113907.

https://doi.org/10.1021/acsami.3c09066
ACS Appl. Mater. Interfaces 2023, 15, 46213−46225